

GSA Data Repository item 2017328

Evidence for melting mud in Earth's mantle from extreme oxygen isotope signatures in zircon

Spencer, C.J.^{1*}, Cavosie, A.J.^{1,2}, Raub, T.D.³, Rollinson, H.⁴, Jeon, H.⁵, Searle, M.P.⁶, Miller, J.A.⁷, EIMF⁸, McDonald, B.J.⁹, Evans, N.J.⁹

¹*The Institute of Geoscience Research (TIGeR), Department of Applied Geology, Curtin University, Perth, Australia*

²*NASA Astrobiology Institute, Department of Geoscience, University of Wisconsin-Madison, Madison, Wisconsin, USA*

³*Department of Earth and Environmental Sciences, University of St Andrews, St Andrews, UK*

⁴*Geoscience, University of Derby, Kedleston Road, Derby, UK*

⁵*Centre for Microscopy, Characterisation and Analysis, University of Western Australia, Crawley, Australia*

⁶*Department of Earth Sciences, University of Oxford, South Parks Road, Oxford, UK*

⁷*Department of Earth Sciences, Stellenbosch University, Stellenbosch, South Africa*

⁸*Edinburgh Ion Microprobe Facility, University of Edinburgh, Edinburgh EH9 3JW, UK*

⁹*GeoHistory Facility, John de Laeter Centre, Department of Applied Geology, Curtin University, Perth, Australia*

Contents

Item DR1: Materials and Methods

Figure DR1: Geochemical data for peraluminous granite in the Oman-UAE ophiolite

Figure DR2: Representative sample photographs

Figure DR3: CL and SE images and ion probe sputter pits of representative samples

Figure DR4: CL and SE images of zircon from sample UAE436

Figure DR5: Information regarding sample-standard bracketing and reproducibility

Figure DR6: Sample-standard bracketing of the $\delta^{18}\text{O}$ map of UAE436_1

Figure DR7: Zircon ϵHf and trace element data

Item DR2: Tabulated data

Table DR1: Normalized Q-A-P (quartz-alkali feldspar-plagioclase feldspar) plots.

Table DR2: GPS locations and data summary

Table DR3: Reference materials data

Table DR4: Summary of zircon $\delta^{18}\text{O}$ data

Table DR5: Oxygen isotope ratio measurements of reference materials

Table DR6: Zircon U-Pb data

Table DR7: Zircon Hf data

Table DR8: Zircon trace element data

Table DR9: Whole rock geochemical data reproduced from Rollinson et al., 2015

Item DR1: Materials and Methods

Sample Descriptions

Samples with 13- and 14- prefix were previously described in detail (Rollinson, 2015). Samples with a UAE- prefix were collected by the British Geological Survey in 2002. UAE15 is a biotite-granite sampled from Wadi Madhah. UAE388 is a muscovite granite sampled south of Al-Dadna. UAE410 is a garnet-bearing biotite granite collected southwest of Bani Hamed. UAE413 is a two-mica granite sampled near Bani Hamed. UAE436 is a biotite granite collected near Al-Bithna. Sample locations are presented in Fig. DR1 and Table DR2. Representative polished slabs and thin section photomicrographs are displayed in Fig. DR2 and DR3. Normalized Q-A-P (quartz-alkali feldspar-plagioclase feldspar) proportions for five UAE samples are displayed in Table DR1.

Zircon separation and imaging methods

Zircon was extracted using standard techniques at Curtin University (i.e. SelFrag, heavy liquid (NaPT and MI), Franz magnetic separation), mounted in epoxy resin and polished to expose a cross section through the centre of the grains. Zircon grains were imaged using cathodoluminescence (CL) and secondary electron (SE) imaging at Curtin University using a MIRA3 field emission scanning electron microscope. Zircon grains from all samples exhibit magmatic zoning patterns (Figs. DR4 and DR5).

Analytical methods for U-Pb/trace element/Hf split stream analysis by LA-ICPMS

Individual zircon grains (mounted and polished in 1" epoxy rounds) were ablated using a Resonetics RESolution M-50A-LR, incorporating a Compex 102 excimer laser. Following a 15-20s period of background analysis, samples were spot ablated for 30 s at a 7Hz repetition rate using a 33 μm beam and laser energy of 1.7 J/cm² at the sample surface. The sample cell was flushed by ultrahigh purity He (0.68 L min⁻¹) and N₂ (2.8 mL min⁻¹). Isotopic intensities were measured using an Agilent 7700s quadrupole ICP-MS and a Nu Instruments Plasma II MC-ICP-MS, with high purity Ar as the plasma gas (flow rate 0.98 L min⁻¹). On the quadrupole, most elements were monitored for 0.01 s each with the exception of ⁸⁸Sr (0.02s), ¹³⁹La (0.04s), ¹⁴¹Pr (0.04s), ²⁰⁴Pb, ²⁰⁶Pb, ²⁰⁷Pb, ²⁰⁸Pb (all Pb 0.03s), ²³²Th (0.0125s), and ²³⁸U (0.0125s).

The primary reference material used for U-Pb dating in this study was 91500 (1062.4±0.4 Ma; Wiedenbeck et al., 1995) with Plesovice (337.13±0.37 Ma; Sláma et al., 2008) used as a secondary age standard. During the analytical session, 91500 yielded a ²⁰⁶Pb/²³⁸U weighted average age of 1062±14 Ma (MSWD = 0.2, n = 10; self-normalized) and Plesovice yielded a ²⁰⁶Pb/²³⁸U weighted average age of 341±3 Ma (MSWD = 0.4, n = 10). ²⁰⁶Pb/²³⁸U ages calculated for Plesovice, treated as unknowns, were found to be within 1% of the accepted value. The time-resolved mass spectra were reduced using the U_Pb_Geochronology3 data reduction scheme in Iolite (Paton et al, 2011 and references therein). Primary reference material used for rare earth elements and titanium was 91500 (Wiedenbeck et al., 1995) with Plesovice (Sláma et al., 2008) used as a secondary reference material. Uncertainties for trace element analysis range between 50% (e.g. La) and 5% (e.g. Yb, Lu). Rare earth element and Ti abundances are typical for crustal zircon (Hoskin and Schaltegger, 2003).

A total of 16 spot analyses were performed on zircon five samples targeting rims and cores. Samples analyzed include 13-24, 14-09, 14-25, 14-29, and UAE413. The number of grains analyzed per sample range from one to six grains.

Half of the split was sent to the MC-ICPMS Lu-Hf isotopic measurement. Masses for ¹⁷²Yb, ¹⁷³Yb, ¹⁷⁵Lu, ¹⁷⁶Hf+Yb+Lu, ¹⁷⁷Hf, ¹⁷⁸Hf, ¹⁷⁹Hf and ¹⁸⁰Hf were measured simultaneously. Reference

zircons Mudtank was used to monitor accuracy and precision of internally corrected (using $^{179}\text{Hf}/^{177}\text{Hf} = 0.7325$) Hf isotope ratios. 91500 and Plesovice were used as secondary standards. During the analytical session, 91500 yielded a corrected $^{176}\text{Hf}/^{177}\text{Hf}$ weighted average ratio of 0.282337 ± 0.000041 (MSWD = 0.2, $n = 8$; self-normalized), Mudtank yielded a corrected $^{176}\text{Hf}/^{177}\text{Hf}$ weighted average ratio of 0.282547 ± 0.000028 (MSWD = 0.3, $n = 8$), and Plesovice yielded a corrected $^{176}\text{Hf}/^{177}\text{Hf}$ weighted average ratio of 0.282506 ± 0.000028 (MSWD = 0.3, $n = 8$). The stable $^{178}\text{Hf}/^{177}\text{Hf}$ and $^{180}\text{Hf}/^{177}\text{Hf}$ ratios for the reference materials yielded values of 1.46709 ± 0.00006 and 1.88682 ± 0.00010 , respectively.

Analytical methods for zircon $\delta^{18}\text{O}$ analysis by SIMS

Zircon oxygen isotopes were measured prior to U-Pb and Hf analyses via secondary ion mass spectrometry (SIMS) using two different SIMS instruments. We used a Cameca 1270 ion microprobe at the Edinburgh Ion Microprobe Facility (EIMF), University of Edinburgh, hereafter referred to as EIMF. We also used a Cameca 1280 microprobe at the Centre for Microscopy, Characterisation and Analysis at the University of Western Australia (CMCA). In general, the analytical methods used for both SIMS instruments are similar to those described previously (e.g., Whitehouse and Nemchin, 2009).

Zircon SIMS analysis for $\delta^{18}\text{O}$ using a 15 μm spot (EIMF and CMCA)

At both Edinburgh and CMCA, the $^{133}\text{Cs}^+$ primary ion beam was accelerated at 10 kV, with an intensity of ~ 2.5 - 3.0 nA current being used, and charge compensation of the Au-coated (30 μm) samples accomplished using a normal incidence electron flood gun. A pre-sputtering time of 30-60 seconds to remove the Au-coat was performed with a projected beam that produced roughly elliptical 15 by 20 μm pits. Ions were extracted with a 10 kV voltage, and low energy secondary ions of ^{16}O and ^{18}O were selected using an energy window of 40 eV or 60 eV (CMCA and EIMF, respectively). During each analysis, the secondary beam was automatically scanned across a small field aperture for centring along the ion-optic axis, followed by scanning the entrance slit across the contrast aperture.

The daily mass resolving power was ~ 2400 , sufficient to resolve hydride interferences (e.g. ^{16}OD , $^{16}\text{OH}_2$). Secondary ions were simultaneously collected on Faraday Cup collectors (FC with different amplifiers of 10E10 and 10E11 ohm resistors, respectively) with average count rates from $2\text{E}9 \pm 1\text{E}8$ cps (1σ) for ^{16}O and $4\text{E}6 \pm 2\text{E}5$ (1σ) cps on ^{18}O . The background of the FC was measured at the beginning of each session during the pre-sputter. Each spot measurement was divided into 2 blocks consisting of 5 or 10 cycles/block (totalling 10 or 20 cycles) with a count time of 4 s/cycle resulting in a total count time of 40 s. Moving the sample, selecting the next grain and area to analyze, pre-sputtering, and ion counting resulted in a total analysis time of approximately 5 min.

Internal precision based on counting statistics is $\sim 5\%$. Total uncertainty values for unknowns are propagated in quadrature to account for external uncertainties (e.g. reference value uncertainty, reference material reproducibility). For this reason, cited uncertainty for unknowns are always larger than the reference materials.

Zircon SIMS analysis for $\delta^{18}\text{O}$ and $^{16}\text{O}^1\text{H}/^{16}\text{O}$ using a ~ 3 μm spot (CMCA)

The sample mount was polished to remove the previous pits, coated with thin Au (10 μm) and then degassed for a week in the IMS-1280 storage chamber. A small Gaussian beam was tuned to make a ~ 3 μm spot, with intensity of ca. 100 pA. A 5 μm rastered beam was used for 60 pre-sputter and then 2 μm raster for the measurement. Smaller field aperture (2000 μm) was used to decrease the electron induced secondary ions from outside of the running spot. Higher mass resolution was achieved to resolve the $^{16}\text{O}^1\text{H}$ peak from ^{17}O , using a narrow entrance slit (60 μm) and exit slit (250 μm ;

resolving power of ca. 5000 by Cameca definition). ^{16}O and OH were collected with FC with an 10E11 ohm resistor, and 18O with electron multiplier (EM) simultaneously. EM high voltage was optimised at the beginning of the session. Each analysis comprised with total 60 cycles (10 cycles x 6 blocks), 4 sec of counting time per cycle. Three zircon reference materials (Temora 2, Penglai, 91500) were measured throughout the whole analyses to check analysis accuracy and precision. The other conditions not mentioned specifically were the same as for the 15 μm beam measurement.

Analyses shown in the $\delta^{18}\text{O}$ map (Fig. 3C) were accompanied with the analysis of $^{16}\text{O}^1\text{H}/^{16}\text{O}$. The $^{16}\text{O}^1\text{H}/^{16}\text{O}$ of the unknowns were normalized to the linear regression of the primary reference material (zircon standards 91500; see Fig. 3C; see also Wang et al., 2014).

Zircon $\delta^{18}\text{O}$ reference materials (15 μm spot analyses, EIMF and CMCA)

For all 15 μm spot analytical sessions, reference materials were analysed in the same mount as the samples, and were used to bracket sample analyses, with approximately 10 sample analyses between each set of reference analyses (Fig. DR5). At EIMF, a total of 71 analyses of an internal reference material (Laura, an in house zircon reference material used at EIMF, $\delta^{18}\text{O}$ by laser fluorination = 5.3‰) were made to calibrate 96 unknown analyses. 91500 (Wiendenbeck et al., 2004) was also analysed 19 times as a secondary reference material. At CMCA, a total of 35 analyses of reference material Laura and Temora 2 was used to calibrate 46 sample analyses. 91500, Penglai (Li et al., 2010), BR266 (Stern, 2001), GJ1 were also analysed 28 times as a secondary reference material. Average analyses for reference materials are given in Table DR3.

Zircon $\delta^{18}\text{O}$ reference materials (3 μm spot analyses, CMCA)

For the 3 μm spot analyses, three zircon standards (91500, Penglai, Temora2) were analysed 32 times and utilized as described above, using the bracketing method. Sample data and full analytical data are given in tables DR4 and DR5. Uncertainties on individual analyses are reported at 1 σ level.

Assessing reproducibility of $\delta^{18}\text{O}$ results from different laboratories

To assess data reproducibility of the 15 μm spot analyses, several samples were analysed during different sessions at the two different laboratories (Fig. DR5). Replicate analyses on multiple sets of different zircon grains from the same samples fall within uncertainty of each other.

Assessing instrumental mass fractionation (IMF)

The instrumental mass fractionation factor (IMF) is corrected using the accepted values for the reference material, which for Laura is $\delta^{18}\text{O}_{\text{VSMOW}} = 5.3\text{‰}$ (measured in-house), and for 91500 is $\delta^{18}\text{O}_{\text{VSMOW}} = 9.89\text{‰}$. Measured isotopic ratios ($^{18}\text{O}/^{16}\text{O}$)_M are normalized by using Vienna Standard Mean Ocean Water compositions (VSMOW), then corrected for the instrumental mass fractionation factor (IMF) using equation 1:

$$(\delta^{18}\text{O})_{\text{M}} = \left(\frac{(^{18}\text{O}/^{16}\text{O})_{\text{M}}}{0.0020052} - 1 \right) * 1000 (\text{‰})$$

$$\text{IMF} = (\delta^{18}\text{O})_{\text{M(standard)}} - (\delta^{18}\text{O})_{\text{VSMOW}}$$

$$\delta^{18}\text{O}_{\text{Sample}} = (\delta^{18}\text{O})_{\text{M}} + \text{IMF}$$

Post-analysis imaging of SIMS pits

Analytical pits were examined using a scanning electron microscope at the Curtin University to assure normal pit shape. Some analyses had irregular analytical spots but yielded $\delta^{18}\text{O}$ analyses

within the same range of other pristine pits (Fig. DR3 and DR4). One of the 3 μm spots on grain UAE436_1 was found to have hit a mineral inclusions (Fig. 3B,C) and was thus excluded.

Fractionation of $\delta^{18}\text{O}$ between zircon and whole rock

Zircon grains in equilibrium with pristine mantle-derived melts have $\delta^{18}\text{O}$ values of $5.3 \pm 0.3\text{‰}$ (Valley et al., 2005). Higher $\delta^{18}\text{O}$ values reflect a component enriched in ^{18}O attributed to assimilation of supracrustal material in the magma from which the zircon crystallized (Cavosie et al., 2005; Valley et al., 2003). Melts that incorporate this supracrustal material offset zircon $\delta^{18}\text{O}$ values accordingly (Valley et al., 1994; Roberts et al., 2013). As the fractionation of $\delta^{18}\text{O}$ in zircon varies in a linear fashion with respect to wt% SiO_2 for igneous rocks at magmatic temperatures (Valley et al., 2005), expected whole rock $\delta^{18}\text{O}$ values were calculated using equation 2:

$$\Delta^{18}\text{O}_{(\text{Zrn-WR})} = \delta^{18}\text{O}_{\text{Zrn}} - \delta^{18}\text{O}_{\text{WR}} \quad \Delta^{18}\text{O}_{(\text{Zrc-WR})} = \delta^{18}\text{O}_{\text{Zrc}} - \delta^{18}\text{O}_{\text{WR}} \\ -0.0612 * (\text{wt. \%SiO}_2) + 2.5$$

Analytical methods for whole rock and quartz $\delta^{18}\text{O}$ analysis

The whole rock oxygen isotope ratio ($^{16}\text{O}/^{18}\text{O}$) for samples was determined in the stable isotope laboratory, Department of Geological Sciences, University of Cape Town using a conventional extraction line (Miller and Harris, 2006) and using ClF_3 as the oxidizing reagent. Liberated O_2 was converted to CO_2 using a hot platinized rod and analysed off-line on a Finnigan Delta XP isotope ratio mass spectrometer in dual inlet mode. Quartz oxygen isotope compositions were determined in the stable isotope laboratory at the University of Lausanne (Sharp, 1990; Vennemann et al., 2001). Between 0.5 to 2 mg of sample was loaded onto a small Pt-sample holder and pumped out to a vacuum of about 10–6 mbar. After preflourination of the sample chamber overnight, samples were individually heated with a CO_2 -laser in 50 mbars of pure F_2 . Excess F_2 is separated from the O_2 produced by conversion to Cl_2 using KCl held at 150°C . Extracted O_2 is collected on a molecular sieve (5\AA) and subsequently expanded into the inlet of a Finnigan MAT 253 isotope ratio mass spectrometer. Both whole rock and quartz oxygen isotope compositions are expressed in standard δ -notation expressed in per mil (‰) relative to VSMOW where $\delta = (\text{R}_{\text{sample}}/\text{R}_{\text{standard}} - 1) \times 1000$ and $\text{R} = ^{18}\text{O}/^{16}\text{O}$. Duplicates of internal quartz standards (MQ at the University of Cape Town and LS-1 at the University of Lausanne) calibrated against NBS28 quartz (Coplen et al., 1983) were run with each batch of samples and used to convert the raw data to the VSMOW scale using the accepted value for NBS28 of 9.64‰ . At the University of Cape Town, the long term 2σ variation in MQ analyses is 0.26‰ ($n=30$), whilst at the University of Lausanne, analyses of NBS28 run at the same time as the quartz analyses gave $9.63 \pm 0.1\text{‰}$ ($n=2$).

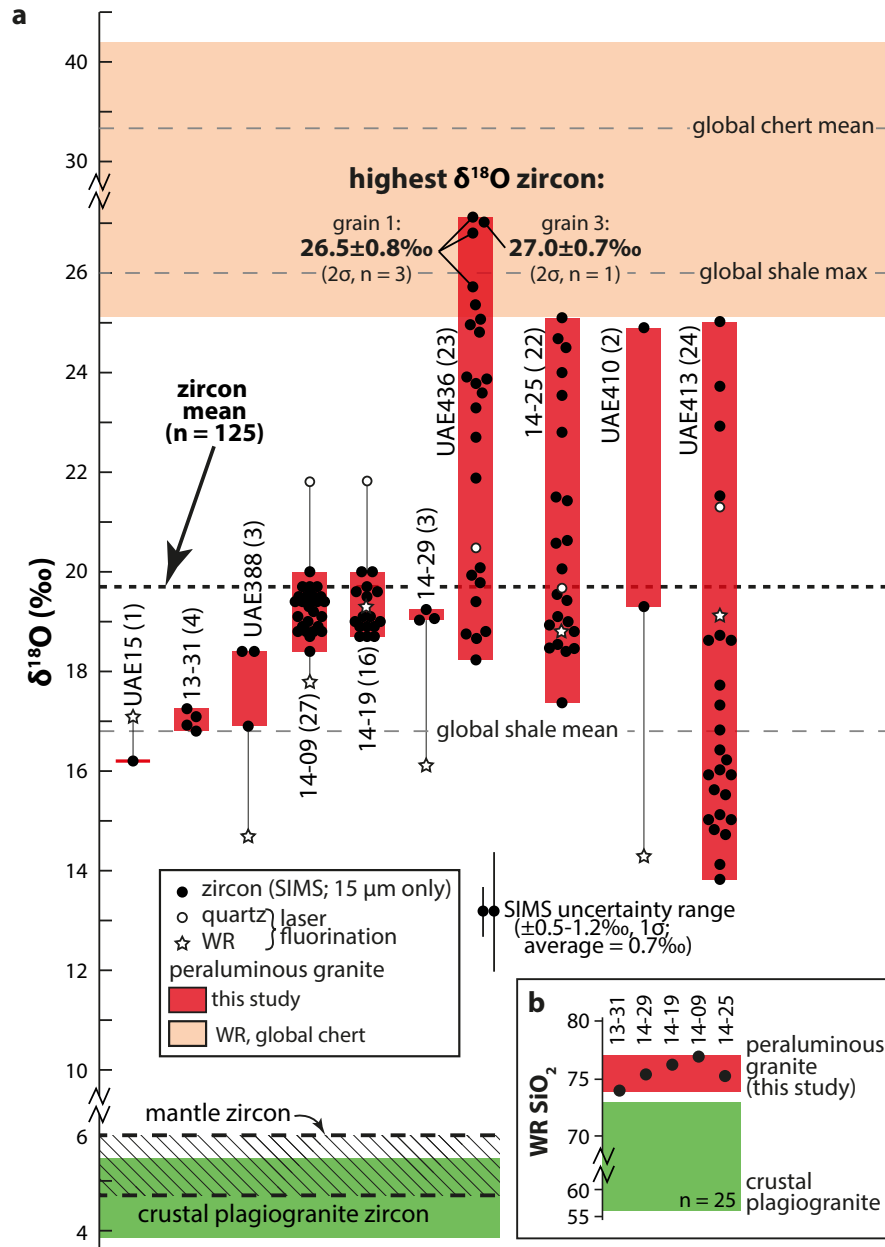


Fig. DR1: Geochemical data for peraluminous granite in the Oman-UAE ophiolite. **a**, Range and mean of zircon, quartz, and whole rock $\delta^{18}\text{O}$ data for peraluminous granite from the Oman-UAE ophiolite. Zircon values are uniformly elevated compared to mantle-equilibrated zircon (Valley et al., 1998) and zircon from crustal plagiogranite in the Oman-UAE ophiolite (Grimes et al., 2013). Parentheses next to sample label indicate number of zircon analyses. Whole rock $\delta^{18}\text{O}$ for Phanerozoic global shale (Payne et al., 2015), chert (Eiler, 2001), and regional marine sediment (Grantham et al., 2003) are shown. The highest $\delta^{18}\text{O}$ values for single zircon grains are indicated (see also Figs. 3 and DR4). WR: whole rock, Qz: quartz, SIMS: secondary ion mass spectrometry, σ : standard deviation. Note breaks in scale. **b**, Whole rock SiO₂ of five peraluminous granite samples analysed for $\delta^{18}\text{O}$ in this study (Rollinson, 2015), showing uniformly higher values compared to crustal plagiogranite (Grimes et al., 2013).

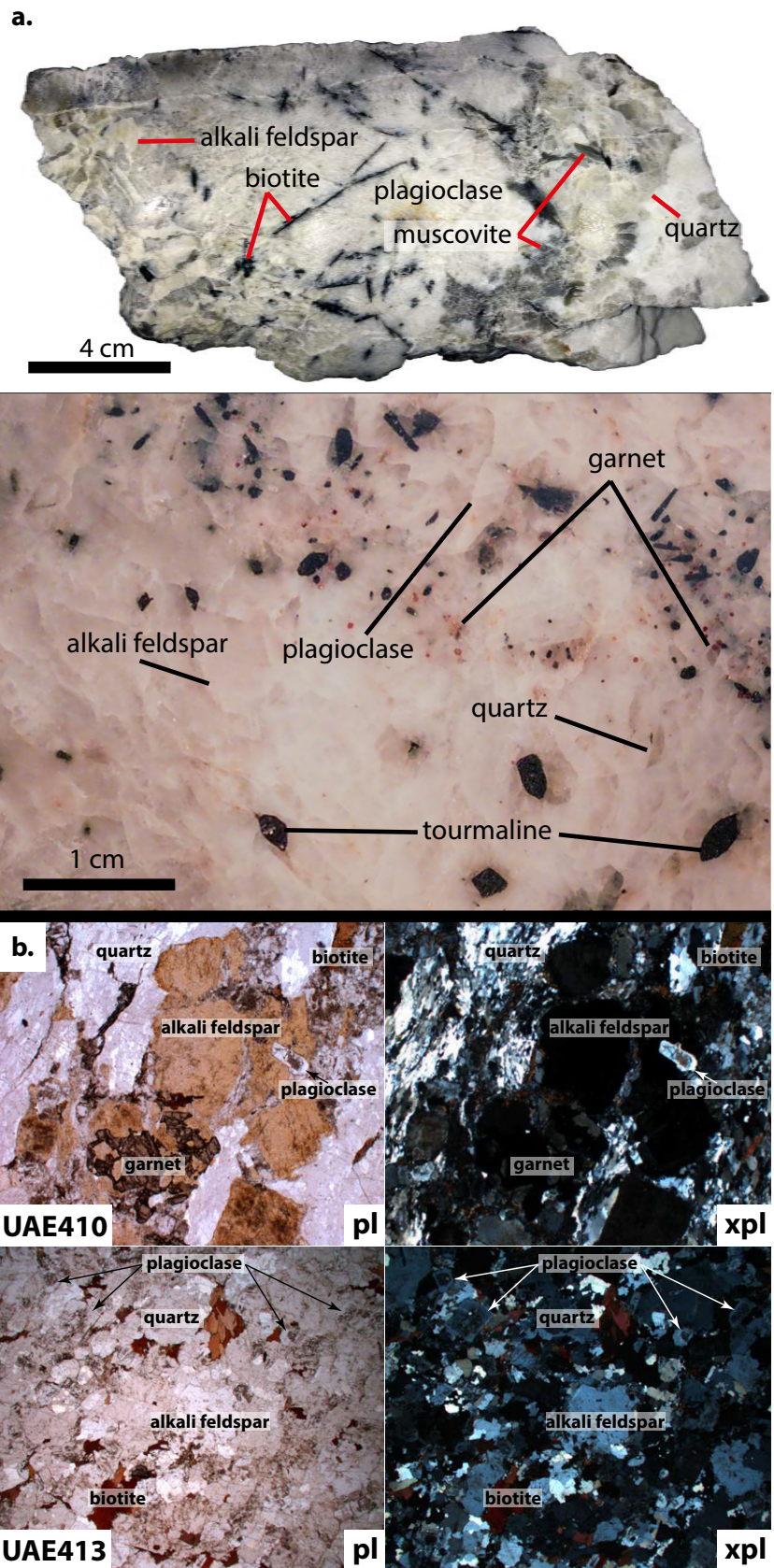


Fig. DR2: **a**, Photographs of granites analysed in this study (samples from site of UAE388). **b**, top) Representative thin section image of sample UAE410. bottom) Representative thin section image of sample UAE413. Plagioclase in many samples exhibit optically dark and inclusion-rich cores with clear euhedral rims, a classic hallmark of S-type granite (2). pl = plain light, xpl = crossed polarized light.

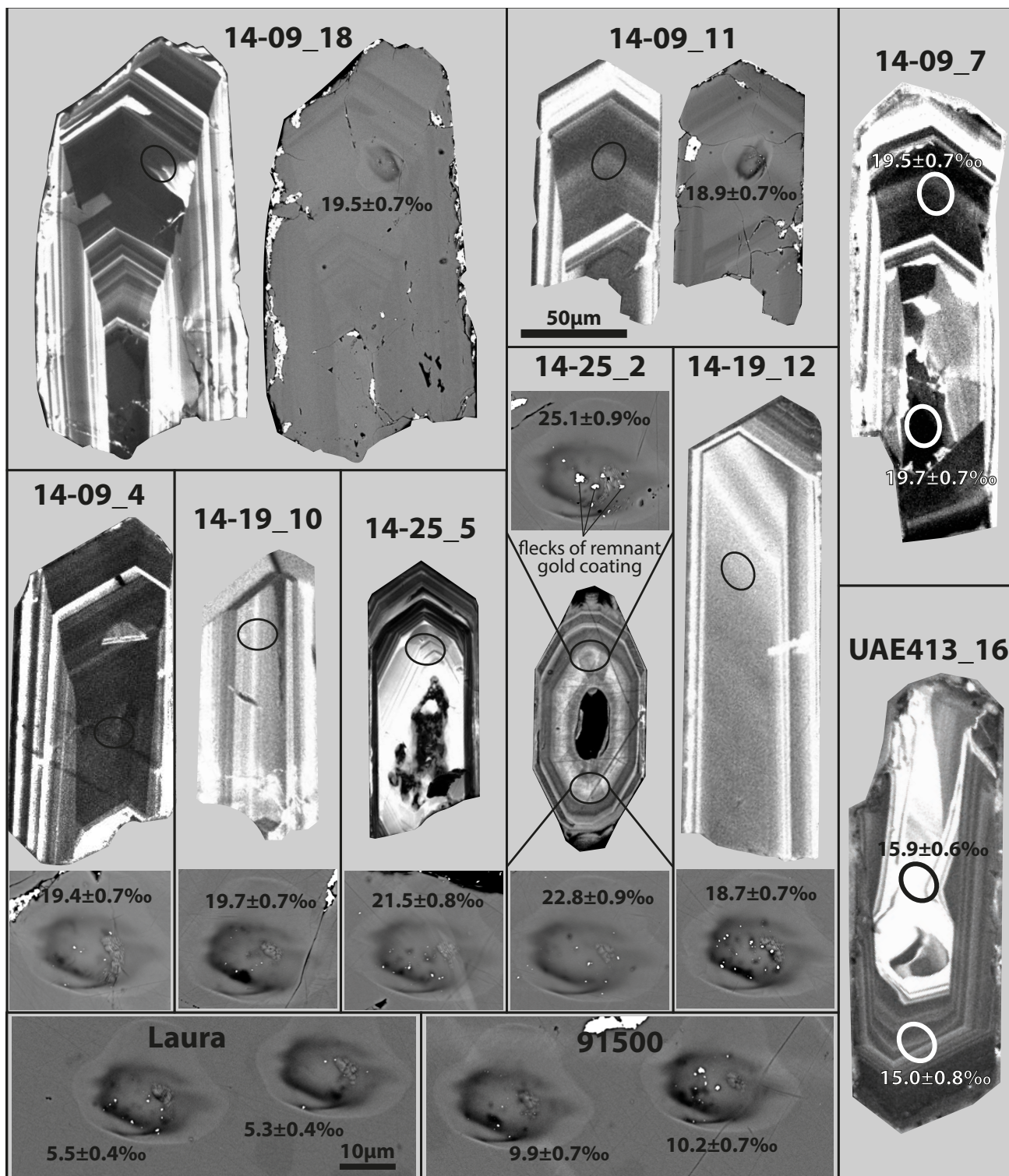


Fig. DR3: CL and SE images and ion probe sputter pits of representative zircon from samples 14-09, 14-19, 14-25, and UAE413. Underscore and number following sample name represents analysis number (Item DR2). The $\delta^{18}\text{O}$ values are displayed next to the analytical spot. Ion probe sputter pits are also included for selected reference materials to illustrate the regular pit appearance (Cavosie et al., 2005). The 15 μm (sputter pits) and 50 μm (zircon grains) scale bars apply to all the respective images.

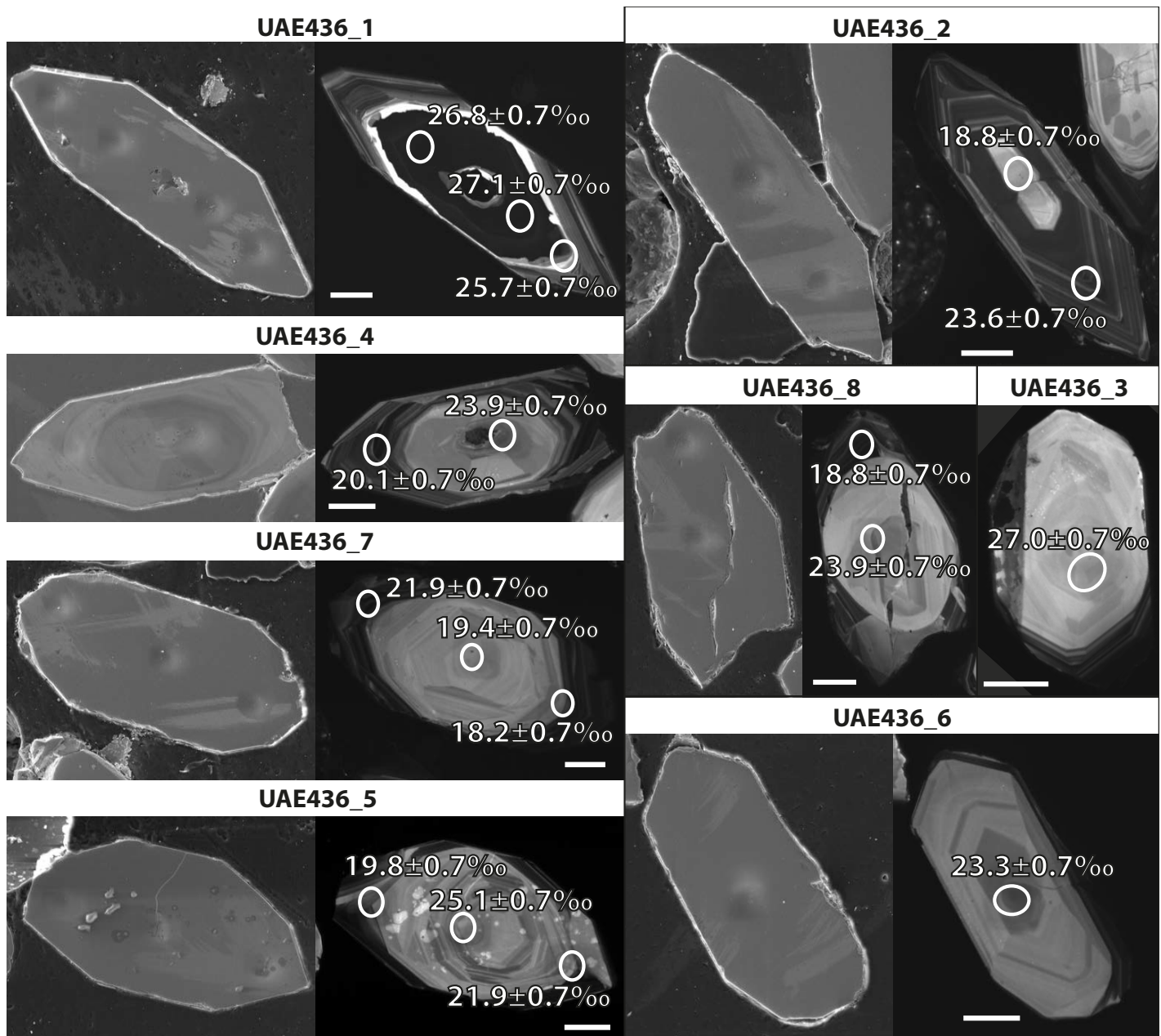


Fig. DR4: CL and SE images of zircon from sample UAE436. Underscore and number following sample name represents analysis number (Item DR2). $\delta^{18}\text{O}$ values are displayed next to the analytical spot. Scale bar for each image is 20 μm .

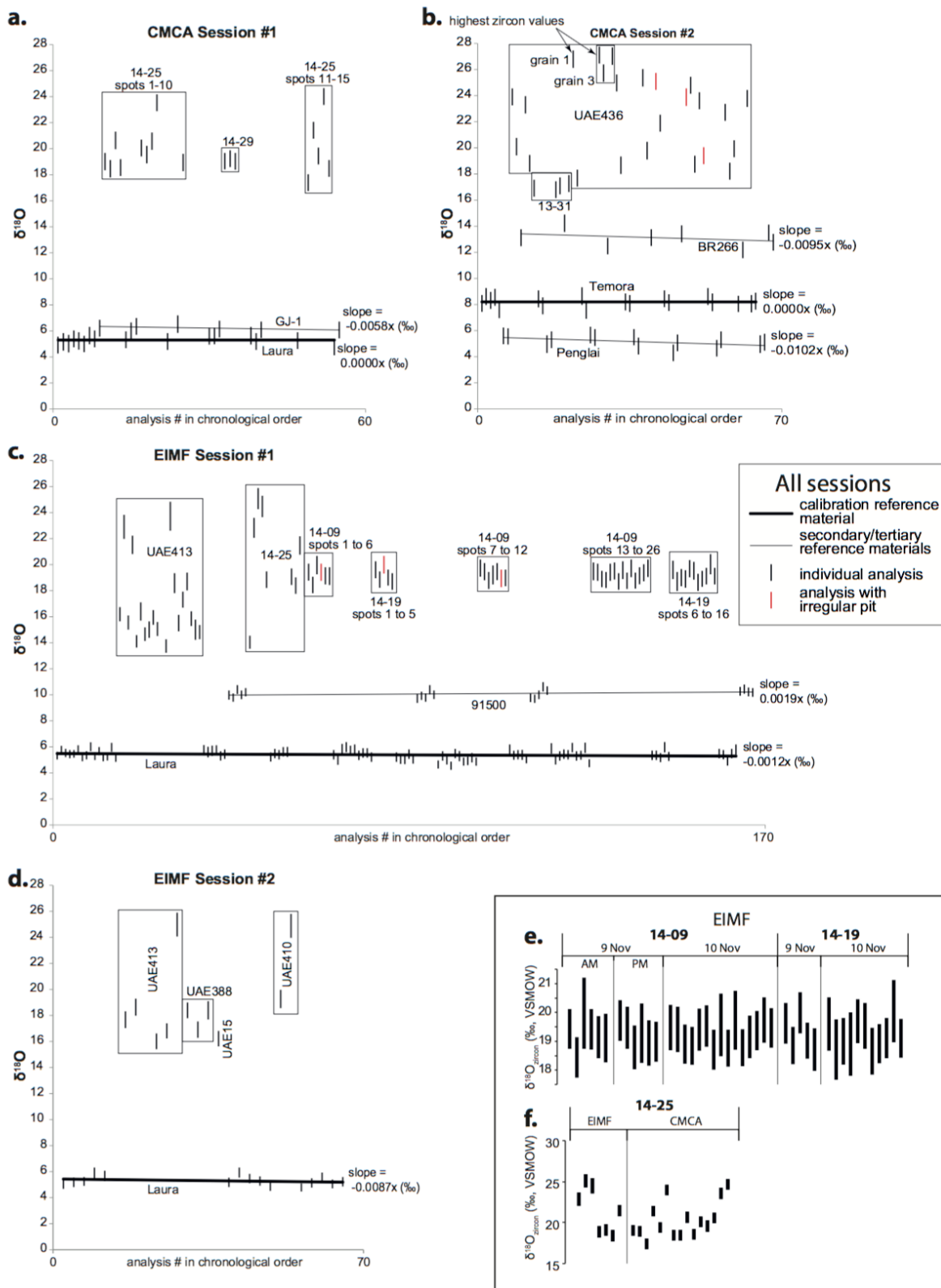


Fig. DR5: a-d, Graphical representation of the analytical bracketing process of reference materials with unknown samples from four analytical sessions at CMCA (**a,b**) and EIMF (**c,d**). All of the analyses are normalized to the calibration reference material indicated. Only the CMCA analytical sessions using 15 μm are represented. Data from the $\sim 3 \mu\text{m}$ are represented in Fig. DR6. The near-zero slope of secondary and tertiary reference materials display the accuracy of the normalization. **e**, Demonstration of data reproducibility of samples 14-09 and 14-19 at EIMF on two separate analytical sessions (including retuning and recalibrating the instrument). **f**, Reproducibility of data for sample 14-25 at EIMF and CMCA using two different secondary ion mass spectrometers, a Cameca ims-1270 and ims-1280, respectively.

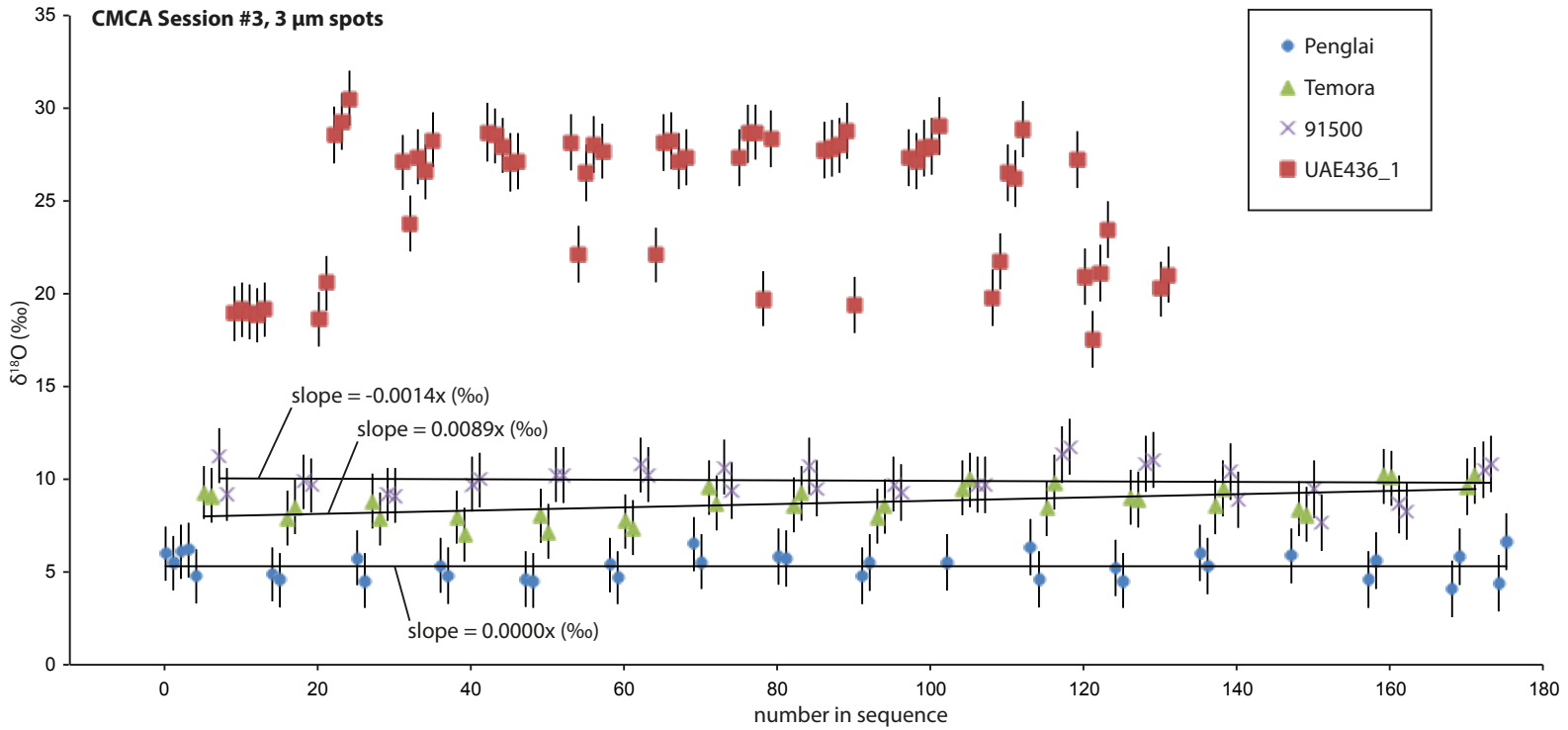


Fig. DR6: Standard-sample-standard bracketing procedure of $\delta^{18}\text{O}$ map displayed in Fig. 3c.

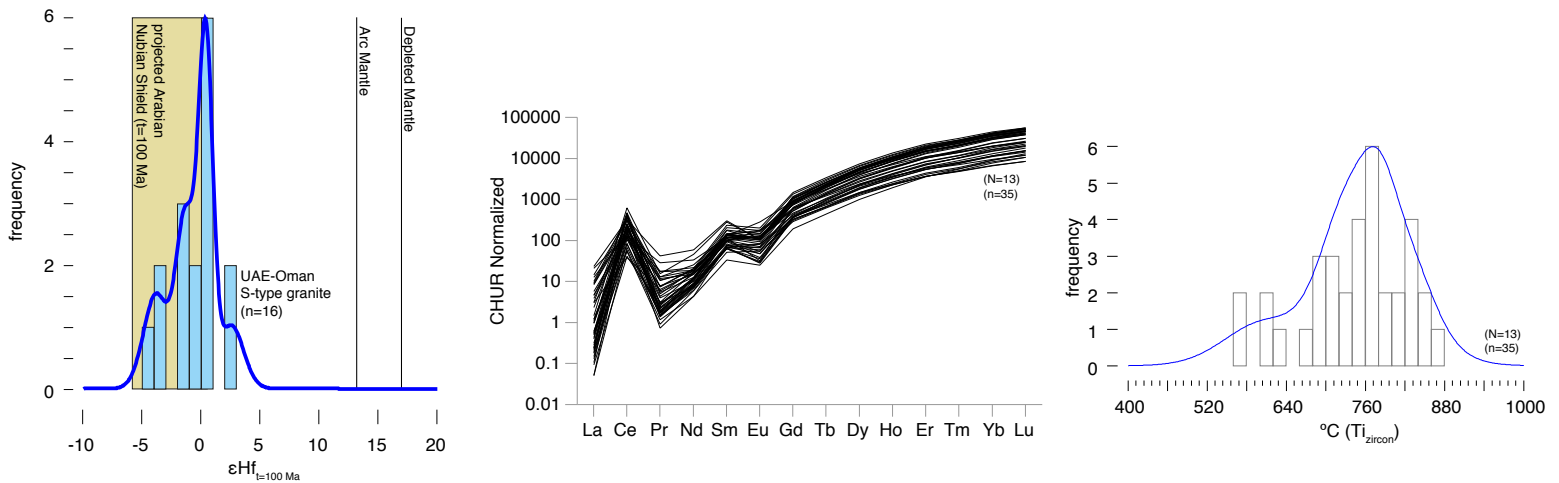


Fig. DR7: Left panel: Combined zircon $\epsilon\text{Hf}_{(t=100)}$ data from this study compared with depleted mantle and arc mantle (Dhuime et al., 2011). Zircon ϵHf data from the Arabian-Nubian Shield (shaded vertical column) are projected assuming a $^{176}\text{Lu}/^{177}\text{Hf}$ ratio of 0.015. Arabian Nubian Shield data compiled from Ali et al., (2012, 2014, 2015a, 2015b, 2015c); Be'eri Shlevin et al. (2010); Morag et al. (2011); Robinson et al., (2014). Center panel: rare earth element chondrite normalized diagram. Right panel: Frequency diagram of Ti-in-zircon temperatures. N = number of samples, n = number of analyses.

Table DR1: Normalized quartz-alkali feldspar-plagioclase feldspar proportions for five samples.
Table DR2: GPS locations and whole rock (WR), quartz (Qz), and zircon (Zrn) data summary with $\delta^{18}\text{O}$ values (‰). n.d. = not determined.
Table DR3: Reference materials $\delta^{18}\text{O}$ weighted averages (wtd avg), two standard deviation uncertainties (2σ), mean square weighted deviation (MSWD), and total number of analyses (n).
Table DR4: Summary of zircon $\delta^{18}\text{O}$ data from individual samples in this study.
Table DR5: Oxygen isotope ratio measurements of reference materials and samples in order of analysis during two sessions at EIMF and two sessions at CMCA.
Table DR6: Zircon U-Pb age data collected via LA-ICPMS.
Table DR7: Zircon Hf age data collected via LA-ICPMS.

References

- Ali, K.A., Kröner, A., Hegner, E., Wong, J., Li, S.-Q.Q., Gahlan, H. a., and Abu El Ela, F.F., 2015, U–Pb zircon geochronology and Hf–Nd isotopic systematics of Wadi Beitan granitoid gneisses, South Eastern Desert, Egypt: *Gondwana Research*, v. 27, no. 2, p. 811–824, doi: 10.1016/j.gr.2013.11.002.
- Ali, K.A., Andersen, A., Manton, W.I., Stern, R.J., Omar, S.A., and Maurice, A.E., 2012, U–Pb zircon dating and Sr–Nd–Hf isotopic evidence to support a juvenile origin of the ~ 634 Ma El Shalul granitic gneiss dome, Arabian–Nubian Shield: *Geological Magazine*, v. 149, no. 5, p. 783–797.
- Ali, K.A., Surour, A.A., Whitehouse, M.J., and Andresen, A., 2015, Single zircon Hf–O isotope constraints on the origin of A-type granites from the Jabal Al-Hassir ring complex, Saudi Arabia: *Precambrian Research*, v. 256, p. 131–147, doi: 10.1016/j.precamres.2014.11.007.
- Ali, K.A., Zoheir, B.A., Stern, R.J., Andresen, A., Whitehouse, M.J., and Bishara, W.W., 2016, Lu–Hf and O isotopic compositions on single zircons from the North Eastern Desert of Egypt, Arabian–Nubian Shield: Implications for crustal evolution: *Gondwana Research*, v. 32, p. 181–192.
- Ali, K.A., Jeon, H., Andresen, A., Li, S.-Q., Harbi, H.M., and Hegner, E., 2014, U–Pb zircon geochronology and Nd–Hf–O isotopic systematics of the Neoproterozoic Hadb adh Dayheen ring complex, Central Arabian Shield, Saudi Arabia: *Lithos*, v. 206–207, p. 348–360, doi: 10.1016/j.lithos.2014.07.030.
- Ali, K.A., Zoheir, B.A., Stern, R.J., Andresen, A., Whitehouse, M.J., and Bishara, W.W., 2015, Lu–Hf and O isotopic compositions on single zircons from the North Eastern Desert of Egypt, Arabian–Nubian Shield: Implications for crustal evolution: *Gondwana Research*, doi: 10.1016/j.gr.2015.02.008.
- Be’eri-Shlevin, Y., Katzir, Y., Blichert-Toft, J., Kleinhanns, I.C., and Whitehouse, M.J., 2010, Nd–Sr–Hf–O isotope provinciality in the northernmost Arabian–Nubian Shield: implications for crustal evolution: *Contributions to Mineralogy and Petrology*, v. 160, no. 2, p. 181–201.
- Cavosie, A.J., Valley, J.W., and Wilde, S. a., 2005, Magmatic $\delta^{18}\text{O}$ in 4400–3900 Ma detrital zircons: A record of the alteration and recycling of crust in the Early Archean: *Earth and Planetary Science Letters*, v. 235, no. 3–4, p. 663–681, doi: 10.1016/j.epsl.2005.04.028.
- Coplen, T.B., Kendall, C., and Hopple, J., 1983, Comparison of stable isotopes reference samples.: *Nature*, v. 302, p. 236–238.
- Dhuime, B., Hawkesworth, C., and Cawood, P., 2011, When continents formed: *Science (New York, N.Y.)*, v. 331, no. 6014, p. 154–5, doi: 10.1126/science.1201245.
- Eiler, J., 2001, Oxygen isotope variations of basaltic lavas and upper mantle rocks, in *Reviews in Mineralogy and geochemistry*, 43.1: 319-364.
- Grantham, G.H., Goedhart, M.L., Wipplinger, R.J., Thomas, R.J., Eglington, B.M., Harmer, R.E., and Hartzler, F.J., 2003, The Surface Geology of the Emirate of Fujairah. Unpublished Report Department of Industry and Economy, Government of Fujairah, United Arab Emirates, 455 pp.
- Grimes, C.B., Ushikubo, T., Kozdon, R., and Valley, J.W., 2013, Perspectives on the origin of plagiogranite in ophiolites from oxygen isotopes in zircon: *Lithos*, v. 179, p. 48–66, doi: 10.1016/j.lithos.2013.07.026.
- Hoskin, P.W.O., and Schaltegger, U., 2003, The composition of zircon and igneous and metamorphic petrogenesis: *Reviews in mineralogy and geochemistry*, v. 53, no. 1, p. 27–62.
- Li, X., Long, W., Li, Q., Liu, Y., Zheng, Y., Yang, Y., Chamberlain, K.R., Wan, D., Guo, C., and Wang, X., 2010, Penglai zircon megacrysts: a potential new working reference material for microbeam determination of Hf–O isotopes and U–Pb age: *Geostandards and Geoanalytical Research*, v. 34, no. 2, p. 117–134.

- Miller, J.A., and Harris, C., 2007, Petrogenesis of the Swaziland and Northern Natal Rhyolites of the Lebombo rifted volcanic margin, South East Africa: *Journal of Petrology*, v. 48, no. 1, p. 185–218, doi: 10.1093/petrology/egl061.
- Morag, N., Avigad, D., Gerdes, A., Belousova, E., and Harlavan, Y., 2011, Detrital zircon Hf isotopic composition indicates long-distance transport of North Gondwana Cambrian-Ordovician sandstones: *Geology*, v. 39, no. 10, p. 955–958, doi: 10.1130/G32184.1.
- Paton, C., Hellstrom, J., Paul, B., Woodhead, J., and Hergt, J., 2011, Iolite: Freeware for the visualisation and processing of mass spectrometric data: *Journal of Analytical Atomic Spectrometry*, v. 26, no. 12, p. 2508–2518.
- Payne, J.L., Hand, M., Pearson, N.J., Barovich, K.M., and McInerney, D.J., 2015, Crustal thickening and clay: Controls on O isotope variation in global magmatism and siliciclastic sedimentary rocks: *Earth and Planetary Science Letters*, v. 412, p. 70–76, doi: 10.1016/j.epsl.2014.12.037.
- Roberts, N.M.W., Slagstad, T., Parrish, R.R., Norry, M.J., Marker, M., and Horstwood, M.S. a., 2013, Sedimentary recycling in arc magmas: geochemical and U–Pb–Hf–O constraints on the Mesoproterozoic Suldal Arc, SW Norway: *Contributions to Mineralogy and Petrology*, v. 165, no. 3, p. 507–523, doi: 10.1007/s00410-012-0820-y.
- Robinson, F.A., Foden, J.D., Collins, A.S., and Payne, J.L., 2014, Arabian Shield magmatic cycles and their relationship with Gondwana assembly: Insights from zircon U–Pb and Hf isotopes: *Earth and Planetary Science Letters*, v. 408, p. 207–225, doi: 10.1016/j.epsl.2014.10.010.
- Rollinson, H., 2015, Slab and sediment melting during subduction initiation: granitoid dykes from the mantle section of the Oman ophiolite: *Contributions to Mineralogy and Petrology*, v. 170, no. 3, p. 1–20.
- Sharp, Z.D., 1990, A laser-based microanalytical method for the *in situ* determination of oxygen isotope ratios of silicates and oxides: *Geochimica et Cosmochimica Acta*, v. 54, no. 5, p. 1353–1357.
- Sláma, J., Košler, J., Condon, D.J., Crowley, J.L., Gerdes, A., Hanchar, J.M., Horstwood, M.S. a., Morris, G. a., Nasdala, L., Norberg, N., Schaltegger, U., Schoene, B., Tubrett, M.N., and Whitehouse, M.J., 2008, Plešovice zircon — A new natural reference material for U–Pb and Hf isotopic microanalysis: *Chemical Geology*, v. 249, no. 1–2, p. 1–35, doi: 10.1016/j.chemgeo.2007.11.005.
- Stern, R.A., 2001, A new isotopic and trace-element standard for the ion microprobe: preliminary thermal ionization mass spectrometry (TIMS) U–Pb and electron-microprobe data: *Radiogenic Age and Isotopic Studies, Geological Survey of Canada*, v. Report 14, p. Current Research 2001-F.
- Valley, J.W., Bindeman, I.N.I., and Peck, W.W.H., 2003, Empirical calibration of oxygen isotope fractionation in zircon: *Geochimica et Cosmochimica Acta*, v. 67, no. 17, p. 3257–3266, doi: 10.1016/S0016-7037(00)00090-5.
- Valley, J.W., Lackey, J.S., Cavosie, A. J., Clechenko, C.C., Spicuzza, M.J., Basei, M. a. S., Bindeman, I.N., Ferreira, V.P., Sial, A. N., King, E.M., Peck, W.H., Sinha, A. K., and Wei, C.S., 2005, 4.4 billion years of crustal maturation: Oxygen isotope ratios of magmatic zircon: *Contributions to Mineralogy and Petrology*, v. 150, no. 6, p. 561–580, doi: 10.1007/s00410-005-0025-8.
- Valley, J.W., Chiarenzelli, J.R., and McLelland, J.M., 1994, Oxygen isotope geochemistry of zircon: *Earth and Planetary Science Letters*, v. 126, no. 4, p. 187–206, doi: 10.1016/0012-821X(94)90106-6.
- Valley, J.W., Kinny, P.D., Schulze, D.J., and Spicuzza, M.J., 1998, Zircon megacrysts from kimberlite: oxygen isotope variability among mantle melts: *Contributions to Mineralogy and Petrology*, v. 133, no. 1–2, p. 1–11.
- Vennemann, T.W., Morlok, A., von Engelhardt, W., and Kyser, K., 2001, Stable isotope composition of impact glasses from the Nördlinger Ries impact crater, Germany: *Geochimica et Cosmochimica Acta*, v. 65, no. 8, p. 1325–1336.
- Wang, X.L., Coble, M.A., Valley, J.W., Shu, X.J., Kouki, K., Spicuzza, M.J., and Sun, T., 2014, Influence of radiation damage on Late Jurassic zircon from southern China: Evidence from *in situ* measurements of oxygen isotopes, laser Raman, U–Pb ages, and trace elements: *Chemical Geology*, v. 389, p. 122–136, doi:10.1016/j.chemgeo.2014.09.013.
- Wiedenbeck, M., Hanchar, J.M., Peck, W.H., Sylvester, P., Valley, J., Whitehouse, M., Kronz, A., Morishita, Y., Nasdala, L., Fiebig, J., Franchi, I., Girard, J.-P., Greenwood, R.C., Hinton, R., et al., 2004, Further Characterisation of the 91500 Zircon Crystal: *Geostandards and Geoanalytical Research*, v. 28, no. 1, p. 9–39, doi: 10.1111/j.1751-908X.2004.tb01041.x.
- Whitehouse, M.J., and Nemchin, A.A., 2009, High precision, high accuracy measurement of oxygen isotopes in a large lunar zircon by SIMS: *Chemical Geology*, v. 261, no. 1, p. 32–42.